Resolving all-order method convergence problems for atomic physics applications

H. Gharibnejad,[1] E. Eliav,[2] M. S. Safronova,[3] and A. Derevianko[1]
[1]*Department of Physics, University of Nevada, Reno, Nevada 89557, USA*
[2]*Department of Chemistry, Tel Aviv University, Tel Aviv, Israel*
[3]*Department of Physics, University of Delaware, Newark, Delaware 19716, USA*
(Received 28 February 2011; published 10 May 2011)

The development of the relativistic all-order method where all single, double, and partial triple excitations of the Dirac-Hartree-Fock wave function are included to all orders of perturbation theory led to many important results for the study of fundamental symmetries, development of atomic clocks, ultracold atom physics, and others, as well as provided recommended values of many atomic properties critically evaluated for their accuracy for a large number of monovalent systems. This approach requires iterative solutions of the linearized coupled-cluster equations leading to convergence issues in some cases where correlation corrections are particularly large or lead to an oscillating pattern. Moreover, these issues also lead to similar problems in the configuration-interaction (CI) + all-order method for many-particle systems. In this work, we have resolved most of the known convergence problems by applying two different convergence stabilizer methods, namely, reduced linear equation and direct inversion of iterative subspace. Examples are presented for B, Al, Zn^+, and Yb^+. Solving these convergence problems greatly expands the number of atomic species that can be treated with the all-order methods and is anticipated to facilitate many interesting future applications.

DOI: 10.1103/PhysRevA.83.052502 PACS number(s): 31.15.bw, 31.15.ac, 06.30.Ft, 31.15.ag

I. INTRODUCTION

The coupled-cluster (CC) method has been successfully applied to solve quantum many-body problems in quantum chemistry [1,2] as well as computational atomic [3] and nuclear physics [4]. A relativistic linearized variant of the coupled-cluster method (which is numerically symmetric and is generally referred to as the "all-order method") was developed for atomic physics applications in Refs. [5–7]. It is one of the most accurate methods currently being used in atomic structure calculations. This approach was extremely successful and led to accurate predictions of energies, transition amplitudes, hyperfine constants, polarizabilities, C_3 and C_6 coefficients, isotope shifts, and other properties of monovalent atoms, as well as the calculation of parity-nonconserving (PNC) amplitudes in Cs, Fr, and Ra^+ (see [8–13] and references therein). Further development of the all-order approach that included triple excitations and nonlinear terms yielded the most precise evaluation of the PNC amplitude in Cs [14,15] and consequent re-analysis of Cs experiments [16]. This work provided the most accurate low-energy test of the electroweak sector of the standard model (SM) to date, placed constraints on a variety of new physics scenarios beyond the SM, and, when combined with the results of high-energy collider experiments, confirmed the energy dependence (or "running") of the electroweak force over an energy range spanning four orders of magnitude (from $\sim$10 MeV to $\sim$100 GeV). The all-order method was also used for the development of ultraprecise atomic clocks [17–21], ultracold atom and quantum information studies [22–26], and many other applications. We refer the reader to review [12] for details of the all-order method and its applications. The all-order method is also used as a part of the configuration-interaction (CI) + all-order approach for the study of more complicated systems [27].

The all-order method requires iterative solutions of the linearized coupled-cluster equations, leading to convergence issues in some cases when correlation corrections are very large or produce an oscillating iterative pattern. The initial guess of the solution is based on the low-order perturbation theory. Therefore, if high-order correlation corrections are large, then the initial guess is very poor, leading to very slow convergence or failure of the straightforward iterative scheme. In addition, initial nonlinear CC equations may have more than one solution, so a convergence to nonphysical solutions may occur. Several such problems have been identified over the years and have led to the failure to apply the all-order approach for many important applications. For example, all or almost all of the low-lying nd and nf states of B, Al, Zn^+, Cd^+, Hg^+, and Yb^+ do not converge if the standard Jacobi-type iterative procedure is applied. In the case of Yb^+, even core equations do not converge. Convergence problems also cause complete failure of the all-order approach for super-heavy elements, such as element 113 (eka-Tl).

All these convergence issues in monovalent systems lead to the same problems in the application of the CI+all-order approach [27] to the corresponding divalent systems, such as Al^+, Hg, Yb, etc., since this method requires the prior solution of linearized coupled-cluster single-double (LCCSD) equations for one-particle orbitals. There are several interesting present applications of these atoms and ions that require high-precision calculations that are possible with all-order techniques. For example, several of these systems are used or proposed for optical clocks [17,28–31] requiring precise knowledge of the blackbody radiation (BBR) shift, which is hard to accurately measure. The BBR shift is a leading source of uncertainties for many of the atomic clock schemes. Yb is used for an ongoing parity nonconservation (PNC) experiment [32], as well as studies of degenerate quantum gases [33,34], due to a number of available isotopes. The best available Yb PNC amplitude value is only accurate to 13% [35].

The convergence issues that arise in the solutions of eigenvalue equations have a long history in general quantum chemistry and several methods have been developed to address

them [36–42]. Most of these methods are based on the fundamental idea of the effective reduction of the original large functional space, and solution of the projected to the reduced (Krylov) subspace of the simplified equations. This idea was implemented in a quantum chemical application by Lanczos [43], who facilitated a partial diagonalization of a large matrix by transforming to a much smaller Krylov subspace, followed by a matrix triangularization procedure.

In the present work, we consider two such convergence techniques, namely, reduced linear equation (RLE) [36,37] and the direct inversion of iterative subspace (DIIS) [38,39]. Both methods use approximate solutions obtained from the few last iterations as Krylov reduced functional subspace onto which the linearized equations are projected and in which the projected system of equations is solved. The convergence of the methods is based on the construction of error vectors. Different choices of the error vectors lead to different implementation of the methods. Among the most popular error vectors are (i) the difference of subsequent iterations, and (ii) the "true" error vector (e.g., the difference between the exact solution and its approximation). In our work, both the convergence methods use the same best least-squares approximation to the true error vector and thus are rather relative. Moreover, our variant of the DIIS method can be regarded as a "symmetric" version of the RLE method (see below). However, while the DIIS method is chosen to minimize the error vector in the least-squares sense, the RLE method differs from it by requiring that this vector within the basis vanishes.

We formulate here implementations of the RLE and DIIS methods for our variant of the coupled-cluster equations, and test these stabilizer methods on several specific examples in which we are able to resolve the convergence problems listed above. We also study the effectiveness of these two techniques in solving specific types of the convergence problems as well as accelerating convergence in all other cases. Acceleration of convergence is particulary important for further CI + all-order use, since it requires solving all-order equations for a large number of one-particle orbitals.

Below, we briefly outline the essence of the convergence stabilization procedures. In the coupled-cluster method, the desired exact wave function $|\psi\rangle$ is obtained by applying (a yet unknown operator) $\exp(T)$ on some reference wave function $|\phi\rangle$, for example, the Dirac-Hartree-Fock (DHF) wave function. For a closed-shell system with N electrons, the cluster operator $T = \sum T_p$ (where $p = 1,2,3,\ldots,N$) has the form

$$T_p = 1/p! \sum_{mn\ldots ab\ldots} \rho_{mn\ldots ab\ldots} a_m^\dagger a_n^\dagger \ldots a_a a_b \ldots . \qquad (1)$$

Here, orbitals $m,n,\ldots$ are single-particle excited states; $a,b,\ldots$ are core states which are occupied in $|\phi\rangle$; ρ's are cluster amplitudes (also called excitation coefficients); and $a^\dagger$ and a are creation and annihilation operators, respectively, with respect to the quasivacuum state $|\phi\rangle$. Finally, p is the number of core electrons that are excited when applying T_p to $|\phi\rangle$. In the LCCSD method, only T_1 and T_2 are retained and nonlinear terms in the expansion of $\exp(T)$ are truncated. The LCCSD equations are conventionally solved by an iterative scheme, symbolically written as $\rho^{(n+1)} = F(\rho^{(n)})$, with F being specified later in Sec. II. In this paper, this type of straightforward iteration procedure is referred to as the conventional iteration scheme (CIS).

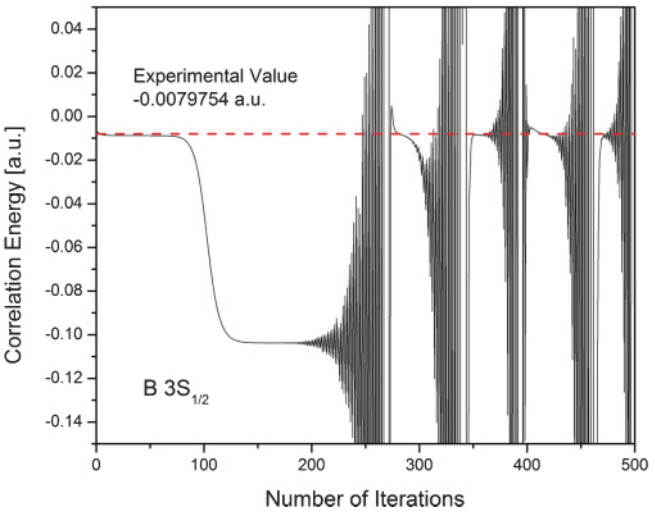

FIG. 1. (Color online) The failure of the LCCSD straightforward iteration procedure for the $3s$ state in boron. The calculated correlation energy is plotted as a function of the iteration number. The dashed (red) line indicates the value of the experimental correlation energy.

Both RLE and DIIS convergence stabilization procedures form the $\rho^{(n+1)}$ solution as the linear combination of cluster amplitudes $[\rho^{(n)},\rho^{(n-1)},\ldots,\rho^{(n-l)}]$ accumulated from l previous CIS iterations. Further details of the LCCSD method and RLE and DIIS schemes are discussed in Secs. II and III.

An example of a failed conventional iteration procedure is shown in Fig. 1, where we plot the LCCSD correlation energy δE as a function of a number of valence LCCSD iterations for the $3s\,^2S_{1/2}$ state of boron. Here and below we treat atoms as if they were monovalent systems. To streamline the notation, we label many-electron states $n\ell_j\,^{2S+1}L_J$ simply as $n\ell_j$ (since $S = 1/2, L = \ell$, and $J = j$). For example, the $3s\,^2S_{1/2}$ state of boron will be labeled as $3s$. The experimental correlation energy ($-0.007\,975\,4$ a.u.) is indicated by the horizontal dashed line. It is computed by subtracting DHF energy from the experimental result. The LCCSD $3s$ correlation energy diverges from the experimental values dramatically and begins to oscillate after a number of iterations. The convergence criteria is set to terminate the iteration procedure when the relative difference between two consecutive iterations is reduced below 0.000 01. The convergence is not reached even after 500 iterations. As demonstrated below, this problem is completely resolved by the use of either RLE or DIIS procedures and convergence to the above criteria is reached within 30 iterations.

This paper is organized as follows. In Sec. II, we describe the LCCSD method and the conventional iteration procedure (CIS) for solving the LCCSD equations. In Sec. III, we formulate RLE and DIIS schemes for LCCSD equations. In Sec. IV, we analyze the performance of the RLE and DIIS schemes for various cases. Finally, in Sec. V, we draw the conclusions.

II. LINEARIZED COUPLED-CLUSTER SINGLE-DOUBLE METHOD

In the present implementation of the CC method, the exact valence wave function $|\psi_v\rangle$ is obtained from the lowest-order DHF state,

$$|\phi_v\rangle = a_v^\dagger|0_c\rangle, \tag{2}$$

by applying a wave operator $\Omega = N[\exp(T)]$ [3],

$$|\psi_v\rangle = \Omega|\phi_v\rangle, \tag{3}$$

where $|0_c\rangle$ is the core DHF state and $N[\cdots]$ designates the normal product of operators with respect to a closed-shell core. Taking into account only the T_1 and T_2 terms in Eq. (1), and truncating Ω past the linear terms in the expansion of the exponential, leads to the LCCSD ansatz for the wave operator:

$$\begin{aligned}\Omega \simeq\ & 1 + \sum_{ma}\rho_{ma}a_m^\dagger a_a + \frac{1}{2}\sum_{mnab}\rho_{mnab}a_m^\dagger a_n^\dagger a_b a_a \\ & + \sum_{m\neq v}\rho_{mv}a_m^\dagger a_v + \sum_{mna}\rho_{mnva}a_m^\dagger a_n^\dagger a_a a_v \\ =\ & 1 + S_c + D_c + S_v + D_v. \end{aligned}\tag{4}$$

Here, S_c and D_c (S_v, D_v) are the core (valence) single and double terms, respectively.

To find the cluster amplitudes (or excitation coefficients) ρ, we need to specify the Hamiltonian. In our approach, we use the Hamiltonian [7] $H = H_0 + G$,

$$H = \sum_i \varepsilon_i N[a_i^\dagger a_i] + \frac{1}{2}\sum_{ijkl} g_{ijkl}N[a_i^\dagger a_j^\dagger a_l a_k], \tag{5}$$

where H_0 is the one-electron lowest-order DHF Hamiltonian and G is the residual Coulomb interaction. Indices i, j, k, and l range over all possible single-particle orbitals, and g_{ijkl} are the two-body Coulomb matrix elements. A set of coupled equations for the cluster operators $(T)_n$, namely,

$$(T_c)_1 = S_c, (T_v)_1 = S_v, (T_c)_2 = D_c, \text{ and } (T_v)_2 = D_v,$$

may be found from the Bloch equation [3]. For monovalent systems [44],

$$(\varepsilon_v - H_0)(T_c)_n = \{QG\Omega\}_{\text{connected},n}, \tag{6}$$

$$(\varepsilon_v + \delta E_v - H_0)(T_v)_n = \{QG\Omega\}_{\text{connected},n}, \tag{7}$$

where $\delta E_v = \langle\phi_v|G\Omega|\phi_v\rangle$ is the valence correlation energy and $Q = 1 - |\phi_v\rangle\langle\phi_v|$ is the projection operator. Note that Eq. (6) contains only the core cluster operators, while Eq. (7) contains both core and valence cluster operators. The core equations (6) are solved first, and the resulting CC core amplitudes are subsequently frozen and used in the valence equations (7).

The summations over the magnetic quantum numbers m in Eqs. (6) and (7) are performed analytically. After the angular reduction, the equation for the reduced, single, core cluster amplitudes $\rho(ma)$ takes the form [9,45]

$$\begin{aligned}&(\varepsilon_a - \varepsilon_m)\rho(ma) \\ &= \delta_{\kappa_m\kappa_a}\left\{\sum_{nb}\delta_{\kappa_n\kappa_b}\sqrt{\frac{[j_b]}{[j_a]}}Z_0(mban)\rho(nb)\right. \\ &\quad - \sum_k\sum_{ncb}\frac{(-1)^{j_a+j_b+j_c+j_n}}{[j_a][k]}Z_k(cbna)\rho_k(nmcb) \\ &\quad \left. + \sum_k\sum_{rnb}\frac{(-1)^{j_a+j_b+j_r+j_n}}{[j_a][k]}Z_k(mbrn)\rho_k(rnab)\right\}. \end{aligned}\tag{8}$$

Here, $[j] = 2j + 1$, κ is the relativistic angular momentum quantum number, $\rho(ma)$ and $\rho_k(mnab)$ are reduced single and double cluster amplitudes, $X_k(mnab)$ are reduced two-body Coulomb matrix elements, and

$$Z_k(mnab) = X_k(mnab) + \sum_{k'}[k]\begin{pmatrix} j_m & j_a & k \\ j_n & j_b & k'\end{pmatrix}X_{k'}(mnba).$$

The equations for the reduced double core cluster amplitudes $\rho_k(mnab)$ are given by

$$\begin{aligned}&(\varepsilon_{ab} - \varepsilon_{mn})\rho_k(mnab) \\ &= X_k(mnab) + \sum_{cd}\sum_{l,k'}A_1X_l(cdab)\rho_{k'}(mncd) \\ &\quad + \sum_{rs}\sum_{l,k'}A_2X_l(mnrs)\rho_{k'}(rsab) \\ &\quad + \left[\sum_r X_k(mnrb)\rho(ra)\delta_{\kappa_r\kappa_a} + \sum_c X_k(cnab)\rho(mc)\delta_{\kappa_m\kappa_c}\right. \\ &\quad \left. - \sum_{rc}\frac{(-1)^{j_c+j_r+k}}{[k]}Z_k(cnrb)\widetilde{\rho}_k(mrac)\right] + \begin{bmatrix} a \leftrightarrow b \\ m \leftrightarrow n\end{bmatrix}, \end{aligned}\tag{9}$$

where A_i are angular coefficients given in [45] and $\varepsilon_{ij} = \varepsilon_i + \varepsilon_j$. The valence equations have exactly the same form as the core equations with the replacement of index a by the valence index v everywhere, and an addition of the valence correlation energy δE_v into the energy difference on the left-hand side, i.e., $(\varepsilon_a - \varepsilon_m)\rho(ma) \longrightarrow (\varepsilon_v - \varepsilon_m + \delta E_v)\rho(mv)$.

Implementation of the RLE and DIIS procedures requires rewriting the equations for the cluster amplitudes in a specific vector form. We introduce the vector notation

$$\mathbf{t} = \begin{pmatrix}\rho(ma) \\ \rho_k(mnab)\end{pmatrix},$$

where $\rho(ma)$ and $\rho_k(mnab)$ are to be understood as columns composed of all amplitudes for single and double excitations, respectively, i.e., for all possible values of m, n, a, b, and k indexes. Then, the core equations given by Eqs. (8) and (9) may be combined as

$$\mathbf{D}\cdot\mathbf{t} = -\mathbf{a} - \Delta\cdot\mathbf{t}, \tag{10}$$

where

$$\mathbf{a} = -\begin{pmatrix}0 \\ X_k(mnab)\end{pmatrix}, \quad \mathbf{D} = \begin{pmatrix}\varepsilon_a - \varepsilon_m \\ \varepsilon_{ab} - \varepsilon_{mn}\end{pmatrix},$$

and $\Delta \cdot \mathbf{t}$ includes all terms on the right-hand sides of Eqs. (8) and (9), except for $X_k(mnab)$ which is included in $\mathbf{a}$.

Valence equations may be written in the same way, with

$$\mathbf{t} = \begin{pmatrix} \rho(mv) \\ \rho_k(mnvb) \end{pmatrix}$$

and

$$\mathbf{a} = -\begin{pmatrix} 0 \\ X_k(mnvb) \end{pmatrix}, \quad \mathbf{D} = \begin{pmatrix} \varepsilon_v - \varepsilon_m + \delta E_v \\ \varepsilon_{vb} - \varepsilon_{mn} + \delta E_v \end{pmatrix}.$$

The main difference between the core and valence equations for the implementation of the RLE and DIIS procedures is the dependence of the valence array D on the iteration number, since δE_v is recalculated after every iteration. In the core case, D remains constant.

Here it should be noted that in $\mathbf{a}$ matrix above, there are additional terms that rise from solutions of cluster amplitudes of the core orbitals. However, because such terms are much smaller than $X_k(mnvb)$ we chose to ignore such terms. Test runs done with the said additional terms showed only minor improvements and the additional terms are computationally expensive.

Solving Eq. (10) for $\mathbf{t}$ gives

$$\mathbf{t} = -\mathbf{D}^{-1}(\mathbf{a} + \Delta \cdot \mathbf{t}). \tag{11}$$

The above equation can be solved iteratively as

$$\mathbf{t}^{(m+1)} = -\mathbf{D}^{-1}(\mathbf{a} + \Delta \cdot \mathbf{t}^{(m)}). \tag{12}$$

The iteration usually starts by inserting $\mathbf{t}^{(0)} = 0$ on the right-hand side of Eq. (12) and finding $\mathbf{t}^{(1)}$. As we demonstrated in Fig. 1, convergence of this straightforward iterative scheme is occasionally very slow or fails altogether. The convergence methods that we develop in the next section will alleviate such problems and lead to faster convergence rates.

III. RLE AND DIIS METHODS

In this section, we formulate the implementation of RLE and DIIS methods for the LCCSD equations (11) discussed in the previous section. Both methods are two-step procedures. In the first step, a few iterative solutions $\mathbf{t}^{(i)}$ of Eq. (12) are found (same as the CIS). In the second step, a linear combination of these $\mathbf{t}^{(i)}$ is used to find the next-best solution of Eq. (12). The new answer is then used for another initialization of the CIS and the two steps are repeated until convergence to specified criteria is reached. In this section, we present the general RLE and DIIS formulas and derive their explicit form for the LCCSD equations.

After accumulating $m+1$ iteratively found solutions, $\mathbf{t}^{(1)}, \mathbf{t}^{(2)}, \ldots, \mathbf{t}^{(m+1)}$, the next-best approximation can be found as their linear combination,

$$\mathbf{t}^{[m+1]} = \sum_{i=1}^{m} \sigma_i \mathbf{t}^{(i)} = \sigma \cdot \mathbf{T}. \tag{13}$$

The quantities σ_i are the weights that have to be determined by solving a system of equations constructed from previously found $m+1$ CIS solutions. We note that $\mathbf{t}^{(m+1)}$ is not included in the linear combination (13), but is used to find σ_i coefficients. Therefore, we use the notation $\mathbf{t}^{[m+1]}$ instead of $\mathbf{t}^{(m+1)}$ to distinguish between the $(m+1)$th solution found through the use of RLE or DIIS methods, and the initial CIS result, respectively.

Both the direct inversion of iterative space (DIIS) and reduced linear equation (RLE) methods seek to minimize the error between the iteratively found solutions of Eq. (11) and the exact answer. The error minimization is the basis for finding the appropriate σ_i to form the approximate solution $\mathbf{t}^{[m+1]}$. Both methods also use a least-squares approach to the error minimization. Since the exact answer is unknown, approximations are used in the minimization process. The approximate solution, as mentioned before, is constructed as a linear combination of a series of iteratively found solutions. The difference between the DIIS and the RLE methods is in the assumptions they make in order to minimize the errors. Further details of the difference between the two methods and derivations of the DIIS or RLE formulas can be found in the Appendix.

We rewrite Eq. (10) as

$$\mathbf{a} + (\Delta + \mathbf{D})\mathbf{t} = \mathbf{a} + \mathbf{B}\mathbf{t} = 0. \tag{14}$$

The DIIS formula for determining σ_i is given by Eq. (A7),

$$\mathbf{T}^T\mathbf{B}^T\mathbf{a} + \mathbf{T}^T\mathbf{B}^T\mathbf{B}\mathbf{T}\sigma = 0. \tag{15}$$

The RLE formula for determining σ_i is given by Eq. (A9),

$$\mathbf{T}^T(\mathbf{a} + \mathbf{B}\mathbf{T}\sigma) = 0. \tag{16}$$

Both Eqs. (15) and (16) can be written as a system of m equations,

$$\boldsymbol{\alpha} + \mathbf{R}\sigma = 0. \tag{17}$$

Solving the above system of equations for σ can be easily done with standard linear algebra methods. The resulting coefficients σ_i are substituted into Eq. (13) to obtain the best new approximate solution $\mathbf{t}^{[m+1]}$.

Next, we write $\mathbf{R}$ and $\boldsymbol{\alpha}$ of Eq. (17) in their explicit forms for the DIIS and RLE methods. Substituting $\Delta - \mathbf{D}$ for $\mathbf{B}$ into DIIS equation (15) yields, for the σ_i,

$$\mathbf{t}^{T(i)}(\Delta + \mathbf{D})^T a + \mathbf{t}^{T(i)}(\Delta + \mathbf{D})^T(\Delta + \mathbf{D})\mathbf{t}^{(i)}\sigma_i = 0.$$

Using Eq. (12), we find that $\Delta \cdot \mathbf{t}^{(i)} = -(\mathbf{D} \cdot \mathbf{t}^{(i+1)} + \mathbf{a})$. The replacement of the dot products involving Δ with ones involving $\mathbf{D}$ yields an explicit form of the DIIS matrix for core orbitals,

$$\begin{aligned} R_{ij} &= \sum_k D_{kk} a_k \left(t_k^{(i+1)} + t_k^{(j+1)} - t_k^{(i)} - t_k^{(j)}\right) + \sum_k (a_k)^2 \\ &\quad + \sum_k D_{kk}^2 \left(t_k^{(i)} t_k^{(j)} + t_k^{(i+1)} t_k^{(j+1)} - t_k^{(i+1)} t_k^{(j)} - t_k^{(i)} t_k^{(j+1)}\right), \\ \alpha_i &= \sum_k a_k D_{kk} \left(t_k^{(i)} - t_k^{(i+1)}\right) - \sum_k (a_k)^2. \end{aligned} \tag{18}$$

The RLE equations for core orbitals are obtained by repeating the same steps as for the DIIS approach, but starting from Eq. (16). The resulting RLE equations for $\mathbf{R}$ and $\boldsymbol{\alpha}$ are

$$\begin{aligned} R_{ij} &= \sum_{kl} t_k^{(i)}(\Delta_{kl} + D_{kl})t_l^{(j)} \\ &= \sum_k \left[t_k^{(i)} D_{kk} t_k^{(j)} - t_k^{(i)} D_{kk} t_k^{(j+1)} - a_k t_k^{(j)}\right], \\ \alpha_i &= \sum_k t_k^{(i)} a_k. \end{aligned} \tag{19}$$

We noted in the previous section that $\mathbf{D}$ depends on the correlation energy δE_v in the case of the valence equations leading to the dependence of $\mathbf{D}$ on the iteration number. Therefore, the substitution $\mathbf{D} \to \mathbf{D}^{(i)}$ must be made to rewrite the DIIS and RLE equations above for the valence orbitals. To derive the final form of the equations, we have to introduce a somewhat arbitrary dot product and normalization definitions. The explicit form of the core RLE equations is obtained by substituting the expressions for $\mathbf{D}$, $\mathbf{a}$, and $\mathbf{t}$ from the previous section into Eq. (19):

$$\begin{aligned} R_{ij} &= \sum_{ma} (\varepsilon_a - \varepsilon_m)\rho^{(i)}(ma)[\rho^{(j)}(ma) - \rho^{(j+1)}(ma)] \\ &\quad + \sum_L \sum_{mnab} \frac{1}{[L]} (\varepsilon_{ab} - \varepsilon_{mn}) \rho_L^{(i)}(mnab) \\ &\quad \times \left[\rho_L^{(j)}(mnab) - \rho_L^{(j+1)}(mnab)\right] - \alpha_i, \\ \alpha_i &= -\sum_L \sum_{mnab} \frac{1}{[L]} X_L(mnab)\rho_L^{(i)}(mnab). \end{aligned} \tag{20}$$

RLE equations for the valence case are given by

$$\begin{aligned} R_{ij} &= \sum_m \left(\varepsilon_v - \varepsilon_m + \delta E_v^{(j)}\right)\rho^{(i)}(mv)[\rho^{(j)}(mv) - \rho^{(j+1)}(mv)] \\ &\quad + \sum_L \sum_{mnb} \frac{1}{[L]} \frac{1}{[j_v]} \left(\varepsilon_{vb} - \varepsilon_{mn} + \delta E_v^{(j)}\right) \rho_L^{(i)}(mnvb) \\ &\quad \times \left[\rho_L^{(j)}(mnvb) - \rho_L^{(j+1)}(mnvb)\right] - \alpha_i, \\ \alpha_i &= -\sum_L \sum_{mnb} \frac{1}{[L]} \frac{1}{[j_v]} X_L(mnvb)\rho_L^{(i)}(mnvb), \end{aligned} \tag{21}$$

where $[L] = 2L + 1$.

The implementation of the RLE and DIIS methods proceeds as follows. In step one, our code makes a limited number, $m + 1$, of LCCSD iterations using the CIS. This is done to find the $m + 1$ series of single and double cluster amplitudes, $\rho^{(i)}(ma)$ and $\rho_L^{(i)}(mnab)$, that are then saved. In step two, a separate subroutine applies the DIIS or RLE equations to these stored cluster amplitudes to find the appropriate $\mathbf{R}$ and $\boldsymbol{\alpha}$ matrices. The m-dimensional linear equation (17) is solved for σ. The next-best solution of the LCCSD equations is then found by substituting σ into Eq. (13). These two steps are repeated until convergence is reached in accordance with a specified criteria. In the next section, we discuss the results of the application of the DIIS and RLE procedures to the solution of the LCCSD equations in the cases that do not converge or converge to nonphysical answers with the conventional iteration scheme.

IV. RESULTS AND DISCUSSION

In this section, we study and compare the convergence characteristics of the DIIS and the RLE methods. We include a number of test cases in four different systems, B, Al, Zn^+, and Yb^+, which have a large number of states that do not converge with the conventional iterative scheme (CIS). We also test the ability of the RLE and the DIIS methods to accelerate convergence in the cases where the CIS does converge. The main purpose of these tests is to provide general guidelines of how to accelerate or to achieve convergence using the RLE and the DIIS methods. The conclusions and observations of this section may be extrapolated to other systems for both all-order and CI + all-order approaches.

The summary of B and Al convergence tests is given in Table I. We find that convergence patterns for two fine-structure multiplet states, for example $3p_{1/2}$ and $3p_{3/2}$ states, are generally very similar. Therefore, we list only $np_{1/2}$ and $nd_{3/2}$ states, with the exception of the $4d$ states of Al. Tests were performed for both states of the multiplet as an additional check, since similar results are expected. The results are given for the $2p_{1/2}$, $3s$, $3p_{1/2}$, and $3d_{3/2}$ states of B and the $3p_{1/2}$, $4s$, $3d_{3/2}$, $4d_{3/2}$, and $4d_{5/2}$ states of Al. The resulting LCCSD correlation energy is listed in the last column of the table in atomic units. The convergence method is specified in the third column. CIS refers to the initial straightforward iteration scheme. RLE5 designates the RLE convergence method with 5 prestored CIS iterations. Similarly, DIIS8 refers to the DIIS convergence scheme with 8 prestored iterations. The fourth column indicates the iteration number at the end of the run. Cases where the maximum number of iterations allowed during the run was reached are marked with an asterisk. In these cases, convergence did not occur. The convergence criteria was set to terminate the iteration procedure when the relative difference between two consecutive iterations is reduced below 0.000 01. The same convergence criteria is used in all valence test runs. Only the core and the $2p$ states of B converge with the CIS. In the case of Al, all nd states do not converge with the CIS. All of the cases in Table I converge with the DIIS8. We note that we did not list the RLE5 and the DIIS5 results for many of the nd states because convergence was not achieved. In the cases where all methods lead to convergence, both the RLE and the DIIS methods have accelerated convergence rates relative to the CIS.

We may draw two general conclusions from our tests as follows:

(1) If a particular LCCSD run converges with the CIS, then the RLE5 appears to be the most efficient method to accelerate the convergence.

(2) If a particular LCCSD run does *not* converge with the CIS, then the DIIS8 or the DIIS9 appear to be the most efficient method to attain and accelerate the convergence.

We note that these two rules are not absolute, but they serve as good initial guidelines. Our further tests on other (much heavier) systems confirmed these guidelines. We note that the RLE5 method is not sufficient to achieve convergence for most of the divergent cases. The only exception in Table I is the $3s$ state of B. However, while the CIS never converges to our standard criteria for the $3s$ state, it nearly converges to the correct result before exhibiting the diverging and

TABLE I. Convergence tests of the LCCSD equations with CIS, RLE, and DIIS methods for B and Al. CIS is the conventional iterations scheme (no convergence stabilizer). RLE5 designates the RLE convergence method with 5 prestored iterations. The last column gives the resulting correlation energy in atomic units.

Atom	State	Method	No. of iterations	Converged?	δE_v(a.u.)
B	Core	CIS	21	Yes	
		RLE5	9	Yes	
		DIIS5	15	Yes	
B	$2p_{1/2}$	CIS	18	Yes	−0.0293907
		RLE5	13	Yes	−0.0293906
		DIIS5	13	Yes	−0.0293908
B	$3s$	CIS	70[a]	No	−0.0091643
		RLE4	70[a]	No	−0.0070438
		DIIS4	70[a]	No	−0.0089454
		RLE5	30	Yes	−0.0089491
		DIIS5	22	Yes	−0.0089472
		DIIS7	31	Yes	−0.0089488
B	$3p_{1/2}$	CIS	44	Yes	−0.0056292
		RLE5	23	Yes	−0.0056294
		DIIS5	19	Yes	−0.0056284
		RLE8	25	Yes	−0.0056295
		DIIS8	24	Yes	−0.0056293
B	$3d_{3/2}$	CIS	85[a]	No	−0.0884489
		DIIS7	71	Yes	−0.0007535
		RLE8	66	Yes	−0.0007536
		DIIS8	51	Yes	−0.0007533
Al	Core	CIS	13	Yes	
		RLE5	8	Yes	
Al	$3p_{1/2}$	CIS	16	Yes	−0.0245810
		RLE5	11	Yes	−0.0245798
		DIIS5	14	Yes	−0.0245811
Al	$4s$	CIS	20	Yes	−0.0079907
		RLE5	13	Yes	−0.0079906
		DIIS5	18	Yes	−0.0079905
Al	$3d_{3/2}$	CIS	70[a]	No	−0.0209573
		DIIS6	89	Yes	−0.0208637
		RLE8	86	Yes	−0.0208662
		DIIS8	49	Yes	−0.0208662
Al	$4d_{3/2}$	CIS	70[a]	No	−0.0213727
		RLE8	300[a]	No	0.0022280
		DIIS8	81	Yes	0.0022478
		DIIS9	91	Yes	0.0022477
Al	$4d_{5/2}$	CIS	70[a]	No	−1.3775005
		RLE8	165	Yes	0.0022737
		DIIS8	97	Yes	0.0022710
		DIIS9	73	Yes	0.0022712

[a]Cases where maximum number of iterations allowed during run was reached.

oscillating pattern of Fig. 1. In this case, accumulation of only five iterations is sufficient. However, in the case of the nd states, the CIS is never close to converging to a correct number and, subsequently, the RLE5 method does not work. Occasionally, the DIIS9 method may achieve convergence where the DIIS8 method would not. The use of an even larger number of stored iterations does not improve convergence or efficiency. DIIS10-DIIS12 runs for the $4d$ states converged to nonphysical answers in two instances, but to correct results in all other cases. The number of iterations varied significantly

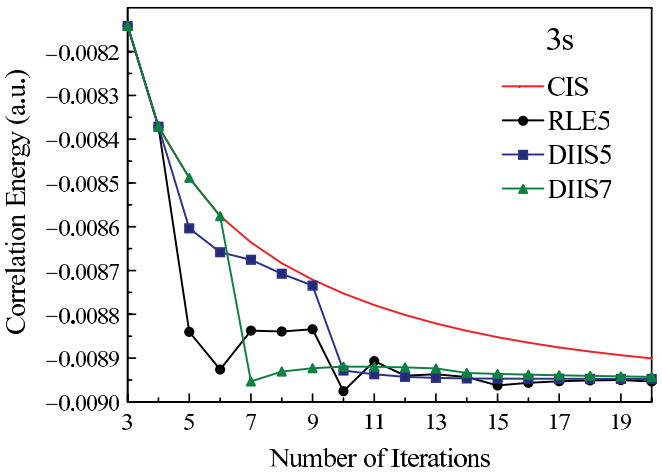

FIG. 2. (Color online) Comparison of the RLE5, DIIS5, and DIIS7 schemes for the $3s$ state of boron. The correlation energy is given in atomic units.

from case to case. The results of all converged runs listed in Table I are consistent within the convergence criteria, as expected.

We implemented the DIIS or RLE strategies for two separately developed LCCSD codes. The calculations were carried out using two different finite basis sets: the B-splines of Ref. [46] and the dual-kinetic-basis sets of Ref. [47]. Even though the basis sets and the convergence criteria used for each code made slight differences in the values, the general observations on the convergence patterns remain the same.

We illustrate the different convergence patterns of the RLE and the DIIS methods for the $3s$ and $3d_{3/2}$ states of boron in Figs. 2 and 3. In Fig. 2, the values of the correlation energies for the $3s$ states of boron are obtained from different schemes that are listed on the graph. RLE5, DIIS5, and DIIS7 results after $N = 20$ interactions are indistinguishable at this plot scale and are not shown. These schemes converge after 30, 22, and 31 iterations, respectively. While the CIS results appear

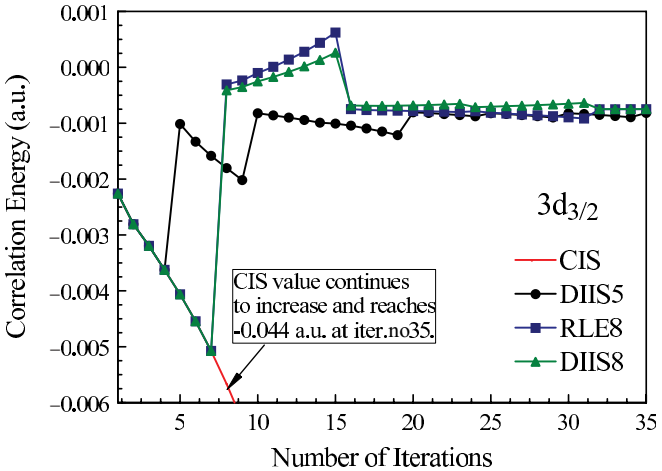

FIG. 3. (Color online) Comparison of the DIIS5, RLE8, and DIIS8 schemes for the $3d_{3/2}$ state of boron. The correlation energy is given in atomic units.

close to the converged value, convergence was never reached and the correlation energy began to oscillate, as illustrated in Fig. 1. The RLE5 and the DIIS5 results are identical to the CIS ones for the first four iterations. The fifth value is different for three of the schemes, as this $(m+1)$th value [see Eq. (13)] is replaced by the RLE or the DIIS predictions for the RLE5 and DIIS5 schemes. We observe that these predictions are significantly closer to the converged result than the fifth CIS iteration. After that, the RLE5 and DIIS5 results are sharply adjusted at $N = 10$ when the second call to the RLE or DIIS stabilizer codes is made. The DIIS7 behavior is similar to the one just described, except that it accumulates seven iterations before the DIIS procedure is invoked, and now the seventh value gets much closer to the final answer.

In Fig. 3, the values of the correlation energies obtained from the CIS, DIIS5, RLE8, and DIIS8 methods are plotted for the $3d_{3/2}$ states of boron. The RLE8 and the DIIS8 results after $N = 35$ appear identical on the graph at this scale and are not shown. The RLE8 and the DIIS8 results converge to our criteria after 66 and 51 iterations, respectively. Very similar behavior of the RLE8 and the DIIS8 results is observed, with the RLE8 energy oscillations being slightly larger after the RLE subroutine pass. However, other tests show that the RLE8 results, in general, converge more slowly, sometimes dramatically so, compared to the DIIS8 results. The CIS values diverge completely and increase rapidly. The DIIS5 results seem to be converging at $N = 35$, but do not in fact reach the selected criteria even after 100 iterations.

The summary of the selected Zn^+ and Yb^+ convergence tests is presented in Table II. The results are given for the $5p_{1/2}$, $4d_{3/2}$, $4d_{5/2}$, and $5d_{3/2}$, $4f_{5/2}$, and $4f_{7/2}$ states of Zn^+, and the Yb^+ core. The $4s$ and $4p_j$ states of Zn^+ and the $6s$, $6p_j$, $7s$, and $5d_j$ states of Yb^+ converge with the CIS results, so we have omitted these results from the table. However, it is worth pointing out that the RLE5 method accelerates convergence for all these states compared to the CIS. Table II demonstrates that the DIIS method reduces the number of iterations for the $5p_{1/2}$ states by a factor of 3 or better. Zn^+ and Yb^+ tests confirm our conclusions (1) and (2), presented earlier in this section. We were unable to achieve convergence for higher $7p_j$ states in Yb^+. This problem is not present in Zn^+, where LCCSD results for the $5p$ states converge even with CIS, as shown in Table II. Perhaps other convergence approaches are needed to resolve this issue.

The case of the Yb^+ core is particularly interesting, since core iterations generally converge well with the CIS. The Yb^+ core is an exception, however, most likely due to very large $4f$ shell contributions that lead to oscillation of the correlation energy. We plot the CIS, the RLE5, and the DIIS5 results for the Yb^+ core correlation energy in Fig. 4. The RLE5 and the DIIS5 results appear identical at this scale and are shown as a single curve. Both methods are successful at fixing the CIS oscillation problem.

The comparison of the B, Al, Zn^+, and Yb^+ removal energies with the experiment from Ref. [48] is given in Table III. The rows labeled "Dif." give the relative difference with experimental values as a percentage. The energies here are given in cm^{-1}. Most of these states did not converge with the CIS, so it is important to establish the accuracy of this approach for such cases. Breit interactions and contributions from higher partial waves are also included. The B and Al ionization potentials, B $2p_{3/2}$ and Al $4s$ single-double (SD) energies, are in agreement with the experiment. We consider only monovalent states for all of these systems. The SD approximation does not account for mixing with the core-excited states, such as $3s3p^2$ in Al. Therefore, larger disagreement with the experiment is expected in the cases

TABLE II. Convergence tests of the LCCSD equations with CIS, RLE, and DIIS methods for Zn^+ and Yb^+. CIS is the conventional iterative scheme (no convergence stabilizer). DIIS8 designates the DIIS convergence method with 8 prestored iterations. The last column gives resulting correlation energy in atomic units.

Atom	State	Method	No. of iterations	Converged?	δE_v(a.u.)
Zn^+	$5p_{1/2}$	CIS	39	Yes	−0.0066119
		DIIS9	12	Yes	−0.0066088
Zn^+	$4d_{3/2}$	CIS	70[a]	No	−0.0977215
		RLE5	67	Yes	−0.0045508
		DIIS8	18	Yes	−0.0045511
Zn^+	$4d_{5/2}$	CIS	70[a]	No	−0.1149058
		RLE5	93	Yes	−0.0045266
		DIIS8	18	Yes	−0.0045267
Zn^+	$5d_{3/2}$	CIS	70[a]	No	−0.1936330
		RLE5	28	Yes	−0.0018929
		DIIS8	18	Yes	−0.0018942
Zn^+	$4f_{5/2}$	CIS	200[a]	No	−0.0008697
		DIIS8	200[a]	No	−0.0007949
		DIIS9	153	Yes	−0.0007948
Zn^+	$4f_{7/2}$	CIS	70[a]	No	−0.0007970
		DIIS8	173	Yes	−0.0007891
		DIIS9	195	Yes	−0.0007891
Yb^+	Core	CIS		No	
		RLE5	12	Yes	
		DIIS5	12	Yes	

[a]Cases where maximum number of iterations allowed during run was reached.

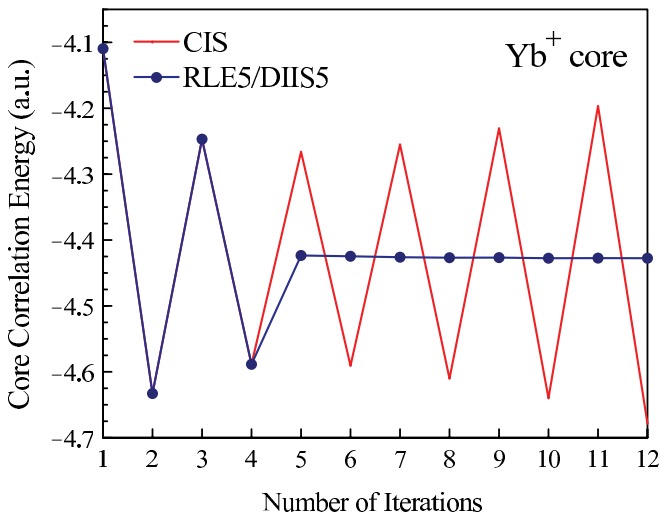

FIG. 4. (Color online) Comparison of the CIS, RLE5, and DIIS5 schemes for the Yb^+ core. The correlation energy is given in atomic units. RLE5 and DIIS5 data appear identical at this scale and are shown as a single curve.

TABLE III. Comparison of B, Al, Zn^+, and Yb^+ removal energies (in cm^{-1}) with experiment [48]. Rows labeled "Dif." give the relative difference with experimental values in percentages (%).

B	$2p_{1/2}$	$2p_{3/2}$	$3s$	$3p_{1/2}$	$3p_{3/2}$	$3d_{3/2}$	$3d_{5/2}$	
Expt.	−66928	−66913	−26888	−18316	−18314	−12160	−12160	
SD	−67049	−67035	−27105	−18497	−18495	−12494	−12494	
Dif.	−0.18%	−0.18%	−0.81%	−0.99%	−0.99%	−2.7%	−2.7%	
Al	$3p_{1/2}$	$4s$	$3d_{3/2}$	$3d_{5/2}$	$4d_{3/2}$	$4d_{5/2}$		
Expt.	−48278	−22931	−15843	−15842	−6045	−6041		
SD	−48271	−23069	−17295	−17289	−6652	−6647		
Dif.	0.02%	−0.60%	−8.4%	−8.4%	−9.1%	−9.1%		
Zn^+	$4s$	$4p_{1/2}$	$4p_{3/2}$	$5p_{1/2}$	$4d_{3/2}$	$4d_{5/2}$	$5d_{3/2}$	$4f_{7/2}$
Expt.	−144691	−96027	−95157	−43360	−47950	−47902	−26913	−27606
SD	−144684	−96221	−95352	−43421	−47929	−47880	−26898	−27633
SDpT	−145232	−96559	−95679	−43492	−47994	−47946	−26929	−27633
Dif. (SD)	0.14%	0.20%	0.19%	0.24%	0.11%	0.11%	0.09%	−0.02%
Dif. (SDpT)	−0.23%	−0.15%	−0.15%	0.08%	−0.02%	−0.03%	−0.02%	−0.01%
Yb^+	$6s$	$6p_{1/2}$	$6p_{3/2}$	$7s$	$5d_{3/2}$	$5d_{5/2}$	$5f_{5/2}$	$5f_{7/2}$
Expt.	−98207	−71145	−67815	−43903	−75246	−73874	−27704	−27627
SD	−98961	−71016	−67480	−44060	−76141	−74700	−28080	−28062
SDpT	−99107	−71084	−67592	−44115	−77764	−76317		
Dif. (SD)	−0.77%	0.18%	0.49%	−0.36%	−1.19%	−1.12%	−1.36%	−1.57%
Dif. (SDpT)	−0.91%	0.09%	0.33%	−0.48%	−3.2%	−3.2%		

where mixing with these one-hole–two-particle states is large. A particular example is the $3d$ and $4d$ states of Al. The lower $3s^2nd$ levels heavily mix with the $3s3p^2\ ^2D$ levels. However, the mixing coefficient for this configuration never exceeds 30%. As a result, these levels are distributed over several lower nd levels, resulting in two sets of levels being listed as $3s^24d\ ^2D$ [48,49], ($[y\ ^2D]$ and $[^2D]$). In Table III, we compare the $4d$ results with the second sets of levels ($[^2D]$).

We also included partial valence triples perturbatively (LCCSDpT) to investigate if the LCCSDpT method would improve the theory-experiment agreement for Zn^+ and Yb^+. This method is described in detail in [9]. Since triple equations are not explicitly iterated in this approach, implementation of the RLE and the DIIS method is exactly the same as in the SD code. Convergence tests of the LCCSDpT method exhibit essentially the same pattern as the tests of the LCCSD method discussed above, and a similar number of iterations was generally required for LCCSD and LCCSDpT calculations for the same states run with the same parameters.

As shown in Table III, we find an excellent agreement of all Zn^+ data with the experiment. The inclusion of perturbative triples somewhat improves the agreement with the experiment for most states. The accuracy decreases for Yb^+, as expected, due to a much softer and heavier core and the strong mixing of monovalent states with one-hole–two-particle states in this system. Nevertheless, for Yb^+, the average accuracy for removal energies is at the level of 1% (see Table III).

V. CONCLUSION

We have successfully implemented the RLE and DIIS convergence techniques in the LCCSD and LCCSDpT methods for high-precision atomic many-body calculations. Most of the convergence problems were resolved using these methods. The acceleration of convergence was demonstrated for all cases where all-order equations converge with the straightforward iteration scheme. Numerous tests were performed to establish general recommendations for the use of the RLE or DIIS methods for various purposes. We find that if a particular case converges with CIS, then the RLE5 method appears to be the most efficient in achieving and accelerating convergence. If a particular case does not converge with CIS, then the DIIS8 or DIIS9 methods appear to be the most efficient in accelerating convergence. Solving these convergence problems greatly expands the number of atomic species that can be treated with the all-order methods and is anticipated to facilitate many interesting future applications for studies of fundamental symmetries, as well as atomic clock and ultracold atom research.

ACKNOWLEDGMENTS

The work of H.G. and A.D. was supported in part by US National Science Foundation Grant No. PHY-9-69580. The work of M.S.S. was supported in part by US National Science Foundation Grant No. PHY-07-58088.

APPENDIX

Derivations of general formulas in this appendix mainly follows the appendix of Ref. [36]. Consider solving a general linear equation of the form

$$\mathbf{a} + \mathbf{Bt} = 0, \tag{A1}$$

which is a system of linear equations of dimension k, with vector $\mathbf{t}$ being the exact solution that we would like to find. We make the best approximation to the exact solution by using $m(< k)$ nonorthogonal and linearly independent vectors

$\mathbf{T} = (\mathbf{t}^{(1)}, \mathbf{t}^{(2)}, \ldots, \mathbf{t}^{(m)})$, where each $\mathbf{t}^{(i)}$ is a k-dimensional vector. We find this best approximation as a linear combination of $\mathbf{t}^{(i)}$'s:

$$\mathbf{t}^{[m+1]} = \sum_{i=1}^{m} \sigma_i \mathbf{t}^{(i)} = \sigma \cdot \mathbf{T}. \tag{A2}$$

Here, σ_i are the weights of the optimized solution that needs to be determined. We note that $\mathbf{t}^{(m+1)}$ is not included in the linear combination (A2), but is used to construct matrices such as those shown in Eqs. (20) and (21). Therefore, $\mathbf{t}^{(m+1)}$ needs to be also found through the CIS. Therefore, we use the notation $\mathbf{t}^{[m+1]}$ instead of $\mathbf{t}^{(m+1)}$ to distinguish between the $(m+1)$th solution found through the use of the RLE or DIIS methods, and the CIS result, respectively.

First, we try to derive an ideal equation to find σ_i's as if we know the exact solution to Eq. (A1). To find the best approximation, we need to minimize the error between the approximate and the exact answers. To this end, we use the least-squares optimization approach. The error is $\mathbf{e} = \mathbf{t} - \mathbf{t}^{[m+1]}$. The least-squares optimization of $E = \mathbf{e}^T\mathbf{e}$ with respect to σ then yields

$$\frac{\partial E}{\partial \sigma} = -2\mathbf{T}^T(\mathbf{t} - \mathbf{T}\cdot\sigma) = 0. \tag{A3}$$

After solving for σ and substituting it into Eq. (A2), we get

$$\mathbf{t}^{[m+1]} = \mathbf{T}(\mathbf{T}^T\mathbf{T})^{-1}\mathbf{T}^T\mathbf{t}. \tag{A4}$$

However, not knowing what the exact solution $\mathbf{t}$ is, the above formula is of little use. The DIIS and RLE methods are based on replacing $\mathbf{t}$ with approximations. Substituting $\mathbf{t}^{[m+1]}$ instead of $\mathbf{t}$ in Eq. (A1) will make Eq. (A1) inhomogeneous:

$$\mathbf{a} + \mathbf{B}\mathbf{t}^{[m+1]} = \mathbf{a} + \mathbf{B}\mathbf{T}\cdot\sigma = \epsilon, \tag{A5}$$

where ϵ is a vector with constant elements.

The difference between the RLE and DIIS methods is in their choice of error to minimize, $\mathbf{e}$. The DIIS method takes the error to be ϵ of Eq. (A5). Then to get the best approximation, we need to minimize $E = \epsilon^T\epsilon$ with respect to σ, as

$$\frac{\partial E}{\partial \sigma} = 2(-\mathbf{B}\mathbf{T})^T(\mathbf{a} + \mathbf{B}\mathbf{T}\sigma) = 0. \tag{A6}$$

Therefore, the coefficients σ that lead to the best approximation satisfy the DIIS equation,

$$\mathbf{T}^T\mathbf{B}^T\mathbf{a} + \mathbf{T}^T\mathbf{B}^T\mathbf{B}\mathbf{T}\sigma = 0\,. \tag{A7}$$

The RLE method requires that the best least-squares approximation $\epsilon^{[m+1]}$ to ϵ vanishes in the space of T. Following the structure of Eq. (A4),

$$\begin{aligned}\epsilon^{[m+1]} &= \mathbf{T}(\mathbf{T}^T\mathbf{T})^{-1}\mathbf{T}^T\epsilon \\ &= \mathbf{T}(\mathbf{T}^T\mathbf{T})^{-1}\mathbf{T}^T(\mathbf{a} + \mathbf{B}\mathbf{T}\sigma) = 0.\end{aligned} \tag{A8}$$

Since $\mathbf{T}$ is made of linearly independent vectors, $\epsilon^{[m+1]}$ is only zero if

$$\mathbf{T}^T(\mathbf{a} + \mathbf{B}\mathbf{T}\sigma) = 0. \tag{A9}$$

Equations (A7) and (A9), for the DIIS and RLE methods, respectively, correspond to Eqs. (15) and (16) in the paper.

[1] J. Čížek, J. Chem. Phys. **45**, 4256 (1966).
[2] R. Bartlett, J. Phys. Chem. **93**, 1697 (1989).
[3] I. Lindgren and J. Morrison, *Atomic Many–Body Theory*, 2nd ed. (Springer–Verlag, Berlin, 1986).
[4] F. Coester and H. Kümmel, Nucl. Phys. **17**, 477 (1960).
[5] S. A. Blundell, W. R. Johnson, Z. W. Liu, and J. Sapirstein, Phys. Rev. A **39**, 3768 (1989).
[6] S. A. Blundell, W. R. Johnson, Z. W. Liu, and J. Sapirstein, Phys. Rev. A **40**, 2233 (1989).
[7] S. A. Blundell, W. R. Johnson, and J. Sapirstein, Phys. Rev. A **43**, 3407 (1991).
[8] S. A. Blundell, J. Sapirstein, and W. R. Johnson, Phys. Rev. D **45**, 1602 (1992).
[9] M. S. Safronova, W. R. Johnson, and A. Derevianko, Phys. Rev. A **60**, 4476 (1999).
[10] A. Derevianko, W. R. Johnson, M. S. Safronova, and J. F. Babb, Phys. Rev. Lett. **82**, 3589 (1999).
[11] M. S. Safronova and W. R. Johnson, Phys. Rev. A **62**, 022112 (2000).
[12] M. S. Safronova and W. R. Johnson, Adv. At. Mol. Opt. Phys. **55**, 191 (2007).
[13] R. Pal, D. Jiang, M. S. Safronova, and U. I. Safronova, Phys. Rev. A **79**, 062505 (2009).
[14] S. G. Porsev, K. Beloy, and A. Derevianko, Phys. Rev. Lett. **102**, 181601 (2009).
[15] S. G. Porsev, K. Beloy, and A. Derevianko, Phys. Rev. D **82**, 036008 (2010).
[16] C. S. Wood, S. C. Bennett, D. Cho, B. P. Masterson, J. L. Roberts, C. E. Tanner, and C. E. Wieman, Science **275**, 1759 (1997).
[17] V. V. Flambaum, V. A. Dzuba, and A. Derevianko, Phys. Rev. Lett. **101**, 220801 (2008).
[18] K. Beloy, U. I. Safronova, and A. Derevianko, Phys. Rev. Lett. **97**, 040801 (2006).
[19] M. S. Safronova, D. Jiang, and U. I. Safronova, Phys. Rev. A **82**, 022510 (2010).
[20] D. Jiang, B. Arora, M. S. Safronova, and C. W. Clark, J. Phys. B **42**, 154020 (2009).
[21] M. S. Safronova, D. Jiang, B. Arora, C. W. Clark, M. G. Kozlov, U. I. Safronova, and W. R. Johnson, IEEE Trans. Ultrason. Ferroelectr. Frequency Control **57**, 94 (2010).
[22] A. Derevianko, Phys. Rev. Lett. **105**, 033002 (2010).
[23] M. J. Morrison, V. A. Dzuba, and A. Derevianko, Phys. Rev. A **83**, 013604 (2011).
[24] B. Ravaine, A. Derevianko, and P. R. Berman, Phys. Rev. A **74**,022330 (2006).
[25] B. Arora, M. S. Safronova, and C. W. Clark, Phys. Rev. A **76**, 052509 (2007).
[26] M. S. Safronova, C. J. Williams, and C. W. Clark, Phys. Rev. A **67**, 040303(R) (2003).
[27] M. S. Safronova, M. G. Kozlov, W. R. Johnson, and D. Jiang, Phys. Rev. A **80**, 012516 (2009).
[28] C. W. Chou, D. B. Hume, J. C. J. Koelemeij, D. J. Wineland, and T. Rosenband, Phys. Rev. Lett. **104**, 070802 (2010).
[29] T. Rosenband *et al.*, Science **319**, 1808 (2008).

[30] V. A. Dzuba and A. Derevianko, J. Phys. B **43**, 074011 (2010).
[31] C. Tamm, S. Weyers, B. Lipphardt, and E. Peik, Phys. Rev. A **80**, 043403 (2009).
[32] K. Tsigutkin, D. Dounas-Frazer, A. Family, J. E. Stalnaker, V. V. Yashchuk, and D. Budker, Phys. Rev. Lett. **103**, 071601 (2009).
[33] V. V. Ivanov, A. Khramov, A. H. Hansen, W. H. Dowd, F. Muenchow, A. O. Jamison, and S. Gupta, e-print arXiv:1101.5142.
[34] S. Tassy, N. Nemitz, F. Baumer, C. Höhl, A. Batär, and A. Görlitz, J. Phys. B **43**, 205309 (2010).
[35] V. A. Dzuba and V. V. Flambaum, Phys. Rev. A **83**, 042514 (2011).
[36] G. D. Purvis and R. J. Bartlett, J. Chem. Phys. **75**, 1284 (1981).
[37] G. W. Trucks, J. Noga, and R. J. Bartlett, Chem. Phys. Lett. **145**, 548 (1988).
[38] P. Pulay, Chem. Phys. Lett. **73**, 393 (1980).
[39] P. Pulay, J. Comput. Chem. **3**, 556 (1982).
[40] N. S. Mosyagin, E. Eliav, and U. Kaldor, J. Phys. B **34**, 339 (2001).
[41] R. J. Harrison, J. Comput. Chem. **25**, 328 (2004).
[42] E. Eliav, M. J. Vilkas, Y. Ishikawa, and U. Kaldor, J. Chem. Phys. **122**, 224113 (2005).
[43] C. Lanczos, J. Res. Natl. Bur. Stand. **45**, 255 (1950).
[44] A. Derevianko and E. D. Emmons, Phys. Rev. A **66**, 012503 (2002).
[45] M. S. Safronova, Ph.D. thesis, University of Notre Dame, 2000.
[46] W. R. Johnson, S. A. Blundell, and J. Sapirstein, Phys. Rev. A **37**, 307 (1988).
[47] K. Beloy and A. Derevianko, Comput. Phys. Commun. **179**, 310 (2008).
[48] J. E. Sansonetti, W. C. Martin, and S. L. Young, *Handbook of Basic Atomic Spectroscopic Data* (NIST, 2006) [http://physics.nist.gov/PhysRefData/Handbook/].
[49] V. Kaufman and W. C. Martin, Phys. Chem. Ref. Data **20**, 775 (1991).